2019-01-0930 Published 02 Apr 2019

Further Experimental Investigation of Motored Engine Friction Using Shunt Pipe Method

Carl Caruana and Mario Farrugia University of Malta

Gilbert Sammut Jaguar & Land Rover, Ltd.

Emiliano Pipitone University of Palermo

Citation: Caruana, C., Farrugia, M., Sammut, G., and Pipitone, E., "Further Experimental Investigation of Motored Engine Friction Using Shunt Pipe Method," *SAE Int. J. Advances & Curr. Prac. in Mobility* 1(4):1444-1453, 2019, doi:10.4271/2019-01-0930.

This article was presented at WCX™19, Detroit, MI, April 9-11, 2019.

Abstract

Mechanical friction is a significant power dissipater in the internal combustion engine. In the effort of designing more efficient and less pollutant engines, friction reduction is certainly on the agenda to be investigated. Such investigation cannot be possible without an accurate measurement of the same quantity. This publication regards a continued study on the mechanical friction determination in an internal combustion engine using the Pressurised Motoring Method. In this work, the friction mean effective pressure of a four-cylinder compression ignition engine was investigated with varying engine speed and manifold pressurisation, using a dedicated high precision sensor for the correct determination of the cylinder Top Dead Centre position. Two different measurement sessions were carried out; in the first, air was employed as pressurisation medium, testing 32 different setpoints; in the second, instead, with the aim to test the effect of the variation of thermochemical properties of fluids on the thermodynamic loss angle, Argon was used in place of air in 18 different setpoints. In the motored condition it is widely accepted that the brake torque is a measure of the losses of the engine and therefore has to be supplied by the driver, in our case the AC motor. The 2000 rpm region was explored with the aim to investigate the high motoring brake torque observed in a previous work from the same authors [1]. An investigation of the volumetric efficiency effect on motoring brake torque is also presented in the paper. Values of IMEP, BMEP, FMEP, peak in-cylinder pressure, loss angle and other parameters are given. The loss angle measured at each setpoint using the TDC sensor is compared with the loss angle evaluated by the use of two thermodynamic methods developed by Stas' [2] and Pipitone [3].

Introduction

Mechanical engine friction is one of the areas in which ongoing research is always present in the hope of maximizing the power output or reducing fuel consumption of the engine through the reduction of parasitic losses. Throughout the years several significant advancements were made in the field, and as Allmaier [4, 5, 6] states, further significant developments need to be done as collective small scale improvements of several components within the IC engine. In order to be able to tackle such small scale improvements, one must have rigorous measurement methods that are able to measure them. As a result of this it would be of benefit to develop new, or reviving existing testing methods in the hope of increasing the measurement accuracy. This publication deals with a continued experimental investigation on the method known as "Pressurized Motoring" or "Motoring with External Charging" in the aim of being used as a tool for developing more accurate FMEP models.

In a previous publication by the same authors [1], a description of the pressurized motoring test rig built at University of Malta was given. Without exhaustively repeating the content of such publication, a small summary of the testing rig built is given here.

The engine used on the test rig is a direct-injection, compression ignition, four cylinder engine with a compression ratio of 18:1. The engine was coupled to an 18kW AC motor. The AC motor was designed to float within a steel framework about its main axis and held from rotating by an S-beam loadcell connected to an arm, which is in turn connected to the motor casing. The motor was powered through a variable frequency drive (VFD), controlled through LabVIEW to be able to change the speed of the engine. A shunt pipe was constructed in between the exhaust collector and the intake manifold in the aim of rerouting the exhausted air. A makeup supply for the previously wasted blow-by was supplied through a single-stage mechanical regulator. A coolant conditioning system was also used in conjunction with a cascade PID controller responsible for the conditioning of the engine oil temperature for steady-state testing.

In this work our intention was to continue the experimental investigation on the Pressurised Motoring method using the same test rig built, with certain changes being done

in the aim of refining over the results acquired in the last publication. The salient points in this work are; the determination of true TDC location using a dedicated probe and the pressurisation of the engine with Argon as well as the observation of its effect on the FMEP and loss angle.

Problem Background

Finding True TDC Location

It is known from literature that 1DegCA error in the TDC location could potentially result in around 10% error in the IMEP [3]. Due to the fact that no TDC probe was available in the tests conducted during the previous work [1], the models developed by Pipitone [3] and Stas' [2] were used in order to determine the thermodynamic loss angle for the motored engine setup at different operating test points. In this work, collaboration was done with University of Palermo in order to assist in the TDC setting of our motored testing rig. Such experimental evaluation of the TDC location was done using a dedicated TDC sensing probe. The TDC location was experimentally evaluated at four different testpoints. Throughout this paper, the testpoints were defined by engine speed and manifold gauge pressure. In all setpoints tested the engine oil temperature was conditioned to be $\mathbf{80^{\circ}C \pm 1^{\circ}C}$. In finding the true TDC position of our engine, the Z-index channel (1 pulse per revolution) of the crankshaft encoder was used as our reference point. This was chosen due to its very good repeatability. It was noted that the angle between the Z-index channel and the peak TDC signal varied by a peak of 0.1DegCA between the setpoints tested, where they ranged from 1100rpm to 1750rpm and from 0.0Bar to 0.5Bar gauge of manifold pressure. Finding the angle at which the peak TDC signal occurs was done by first sectioning the signal to 2DegCA around the peak. In such region some noise was present, with some cycles being worse than others. In order to have a reliable calibration, the cycles were individually compiled and those which were found to be heavily affected with noise were discarded. To the chosen clean cycles, a second order polynomial was then fitted to smoothen the signal and the peak was found relative to the Z-index channel.

From the same data containing both the TDC signal and in-cylinder pressure, the thermodynamic loss angle was calculated as given in Table 1 together with its standard deviation.

It should be noted that results listed in this publication were all computed and averaged over three hundred consecutive cycles, unless otherwise stated. The standard deviation seen in Table 1, is known to originate mainly from two sources; the location of peak pressure and the location of minimum volume as given by equation 1. The location of minimum volume was found from the dedicated TDC probe as already stated, whereas the location of maximum pressure was found from the in-cylinder pressure trace acquired by the piezoelectric pressure sensor. The standard deviation at the tested setpoints of the TDC location is given in Table 2 and the standard deviation of the location of peak pressure is given in Table 3.

TABLE 1 The thermodynamic loss angle relationship with engine speed and load.

Thermodynamic Loss Angle [Deg]		Manifold Gauge Pressure [Bar]	
		0.0	0.5
Engine Speed [RPM]	1100	−1.1 ± 0.3	N/A
	1400	−1.0 ± 0.2	−0.8 ± 0.2
	1750	−0.9 ± 0.2	N/A

TABLE 2 The standard deviation on the TDC location with engine speed and load.

TDC Location Standard Deviation [Deg]		Manifold Gauge Pressure [Bar]	
		0.0	0.5
Engine Speed [RPM]	1100	±0.1	N/A
	1400	±0.1	±0.1
	1750	±0.1	N/A

TABLE 3 The standard deviation of the location of peak pressure with engine speed and load.

LPP Standard Deviation [Deg]		Manifold Gauge Pressure [Bar]	
		0.0	0.5
Engine Speed [RPM]	1100	±0.3	N/A
	1400	±0.2	±0.2
	1750	±0.2	N/A

$$\delta_{\substack{Loss \\ Angle}} = \sqrt{\left(\delta_{\substack{TDC \\ Location}}\right)^2 + \left(\delta_{LPP}\right)^2} \quad \ldots \quad (1)$$

Having obtained the calibration of the true TDC position of the engine, two testing sessions were done. One testing session used air as the pressurization gas, whereas the other used Argon. In compiling the data acquired from these tests, the true TDC position as found from the described previous tests was used.

Argon Pressurisation

In order to investigate the thermochemical effects of different fluids on the thermodynamic loss angle and FMEP, modifications to our test rig were done by which the engine could be operated on both Argon and Air separately, with changeover being a matter of few minutes.

The modifications started by rerouting the engine breathers to the engine intake manifold for reconsumption. In the previous study [1] the engine breather was allowed to dispose of the blow-by gases, however with using a gas like Argon, it was deemed necessary to reroute the blow-by gases to the intake manifold in order to eliminate wastage of the comparatively expensive gas. To achieve this, a reciprocating refrigeration compressor was used, driven by a three phase motor. The compressor inlet was connected to the engine breather outlet through a buffer tank and an orifice plate setup. The buffer tank was used as a reservoir to dampen engine

pulsations as well as serving as an oil trap. The orifice plate setup was used for the purpose of engine blow-by flow rate measurement. The outlet of the compressor was connected to the engine manifold through another oil trap reservoir. This was done to ensure that no refrigerant oil from the compressor ends up in the engine manifold. Just downstream of the oil trap a tee-off was constructed and connected to a normally-closed electronic 1/4 inch valve whose outlet port was reduced to around ∅2mm by a reducing bush for depressurization purposes. Figure 1 shows a schematic representation of the modified setup.

In order to maintain an adequate and stable crankcase pressure, the three phase motor coupled to the compressor was driven through a variable frequency drive (VFD) which in turn was controlled through a LabVIEW PID controller as a function of crankcase pressure measurement. For such measurement an NXP MPXV7007DP pressure sensor was installed in the buffer tank upstream of the compressor inlet port. By this system the speed of the compressor was varied in order to obtain the required crankcase pressure at different engine speed and load setpoints. During testing, the crankcase pressure was always set to around 4kPa above atmospheric conditions in order to ascertain that if a leak was present in one of the engine's gasket, it would be from the engine to the atmosphere and not in the reverse direction, which could possibly dilute the Argon system with air. It must be clear to the reader that such a system had to be PID controlled due to the fact that different engine speeds and loads impose different blow-by flow-rates. This implies that the compressor needs to work at different rates, depending on the blow-by flow rate in order to maintain a steady crankcase pressure.

Prior starting any Argon testing the engine had to be purged using the electronic 1/4inch valve to ascertain that no oxygen was present in the system. To check this, a Uni-NOx sensor sponsored by Continental Corporation was installed in the buffer tank. Such sensor gives an indication of both NOx and O_2 concentration, thus the O_2 reading was constantly monitored. During purging it was seen that the O_2 dropped slowly to around 0%. When such a mark was reached, testing with Argon commenced.

FIGURE 1 A schematic representation of the pressurized motoring setup

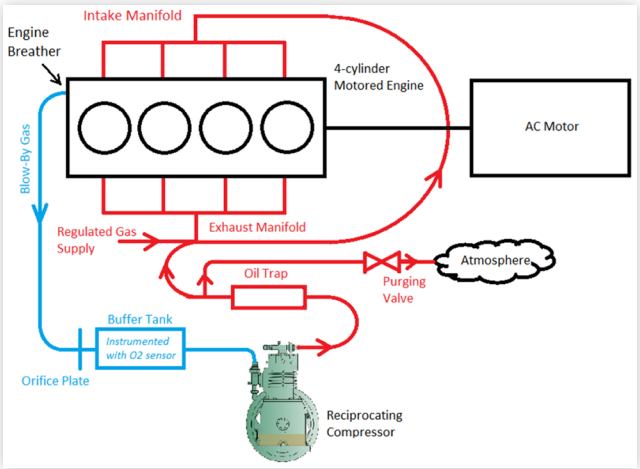

Experimental Testing

Testing with Air

Prior testing with Argon, some time was dedicated to repeat the tests with Air as done in the previous work [1]. There were two motives for this. The first was to investigate the peak motoring brake torque seen at around 2000rpm in the previous work. The second motive was to compare the FMEP trace obtained in this work, using the IMEP computed from the probe determined loss angle to that obtained in the previous work using the IMEP computed from empirical models.

In order to investigate better the peak torque seen at the 2000rpm, the test matrix was extended on the engine speed axis to include finer graduations around the 2000rpm mark, namely 1750rpm and 2250rpm. Apart from this, two additional loading conditions were also tested across the engine speed range. The additional loading conditions were 0.5Bar vacuum and no manifolds condition. The latter loading condition was aimed at identifying whether the anomalies seen at 2000rpm truly originated from the volumetric efficiency as postulated in the previous work [1]. Table 4 shows the planned test matrix.

During such testing, two DAQ systems were used; a slow one with a frequency of 10Hz and a fast one which is externally sampled according to a 0.1DegCA crankshaft encoder. The slow DAQ system was used to record steady-state measurements, such as shunt pipe temperatures, engine speed, manifold pressure, blow-by flow rate and others. Figure 2 shows measurements from two k-type thermocouples, one at the exhaust side of the shunt pipe and one at the intake side. In this study the shunt pipe was unlagged. As seen from Figure 2, the temperature difference between the intake and exhaust side at a particular manifold pressurization seem to get further apart by increasing engine speed.

In order to maintain the oil temperature at $\mathbf{80^{\circ}C}$, the coolant temperature had to be tuned accordingly by the PID controller. It should be mentioned that in this study, the oil temperature was measured in the sump, using a k-type thermocouple. Figure 3 shows the coolant temperatures reached during this testing session.

In the previous publication it was hypothesized that the peak in BMEP seen at the 2000rpm was due to volumetric efficiency effects. Such hypothesis was based on the fact that the peak incylinder pressure also showed large values at the

TABLE 4 The planned test matrix for air testing

		Gauge Pressure [Bar]						
Setpoints Tested		-0.5	0.0	No Manifolds	0.5	1.0	1.5	2.0
Engine Speed [RPM]	1100	✓	N/A	✓	N/A	N/A	N/A	N/A
	1400	✓	✓	✓	✓	✓	✓	N/A
	1750	✓	✓	✓	✓	✓	✓	✓
	2000	✓	✓	✓	✓	✓	✓	N/A
	2250	✓	✓	✓	✓	✓	✓	N/A
	2500	✓	✓	✓	✓	✓	✓	N/A
	3000	✓	✓	✓	✓	✓	✓	N/A

© 2019 SAE International. All Rights Reserved.

FIGURE 2 The graph of shunt pipe intake and exhaust temperatures.

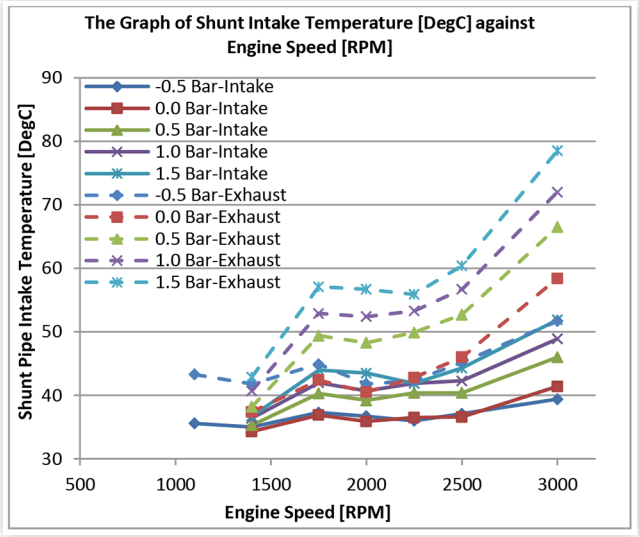

FIGURE 3 Engine coolant temperature at different engine speeds and loads

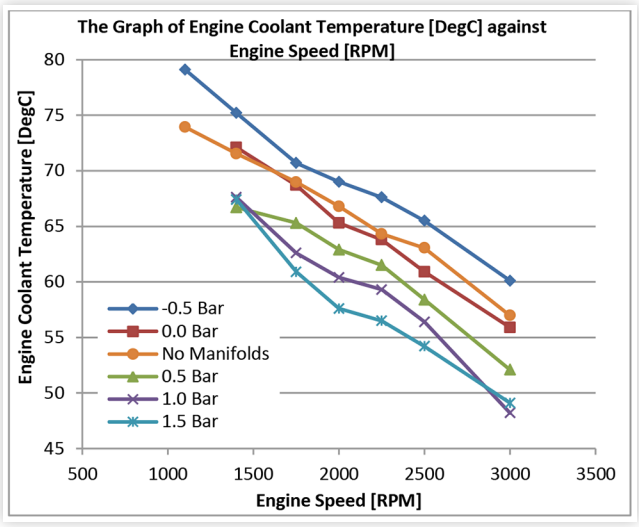

2000rpm region compared to other speeds at the same manifold pressure. Figure 4 shows the peak incylinder pressure at different setpoints for the testing session covered in this work. It can be seen that the 2000rpm gives higher peak pressures on all loads, however comparing the case of no manifolds with that of 0.0Bar gauge, one can see that on the former no peak is seen at the 2000rpm. It should be noted that such two loading conditions are relatively the same with respect to loading; however the one without the manifolds should reduce the dependency on the volumetric efficiency.

Figure 5 shows the BMEP, as obtained from the motoring brake torque recorded at different engine speeds and loads. It is seen that a peak over the 2000rpm is very well evident, as seen in the previous publication [1]. Such behavior was also noted in the IMEP trace in Figure 6. In order to understand better the origin of such behavior, it was thought to be of interest to split the $IMEP_{net}$ into $IMEP_{gross}$ and pumping mean effective

FIGURE 4 The peak in-cylinder pressure at different testpoints

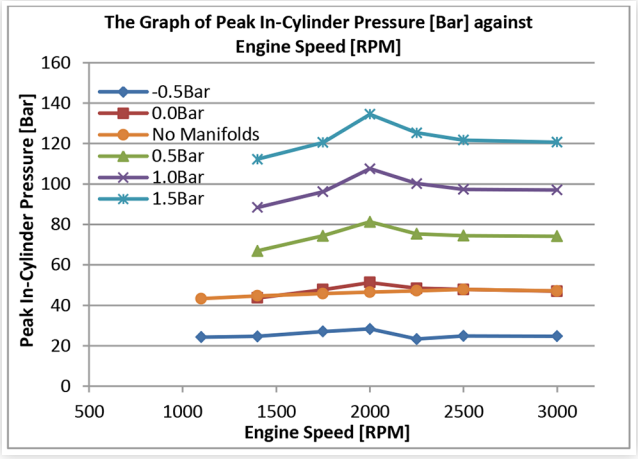

FIGURE 5 The graph of BMEP acquired at different engine speed and load testpoints.

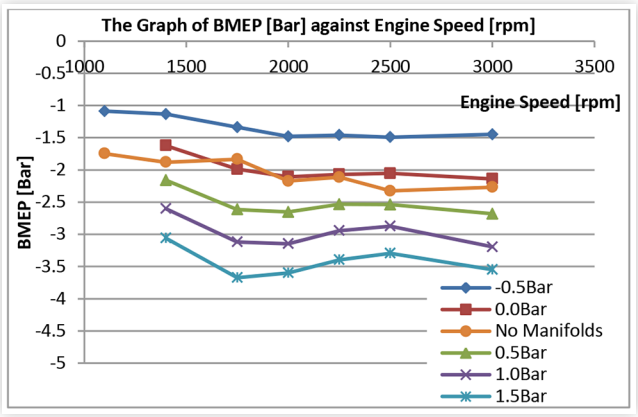

FIGURE 6 The graph of $IMEP_{net}$ against engine speed and load

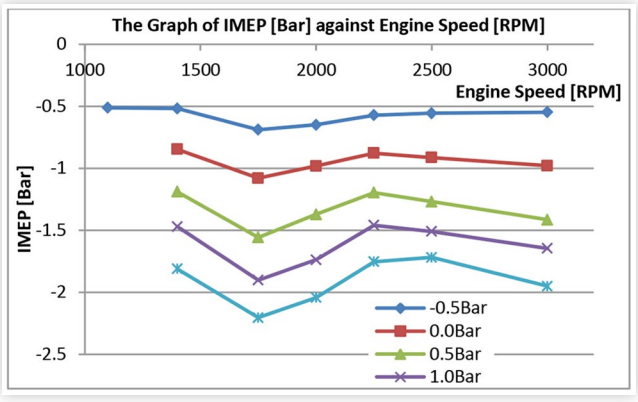

pressure, *PMEP*. Such results are shown in Figure 7 and Figure 8 respectively. It is clear that the graph of $IMEP_{gross}$ resembles a near linear variation (apart from experimental error and complex in-cylinder heat transfer phenomena), whereas the PMEP shows a peak at the 2000rpm, which when superimposed on the $IMEP_{gross}$ yields the shape of the $IMEP_{net}$. Such

FIGURE 7 The graph of $IMEP_{gross}$ against engine speed and load

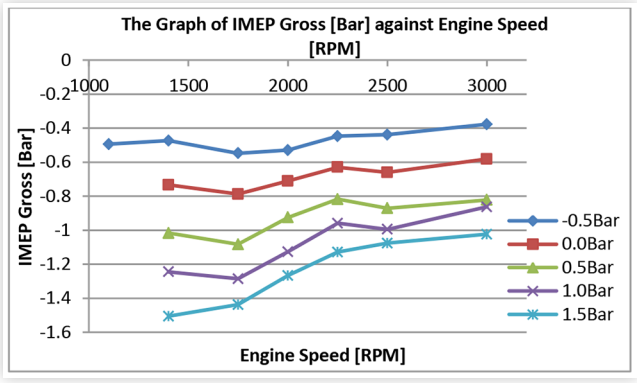

FIGURE 8 The graph of PMEP against engine speed and load

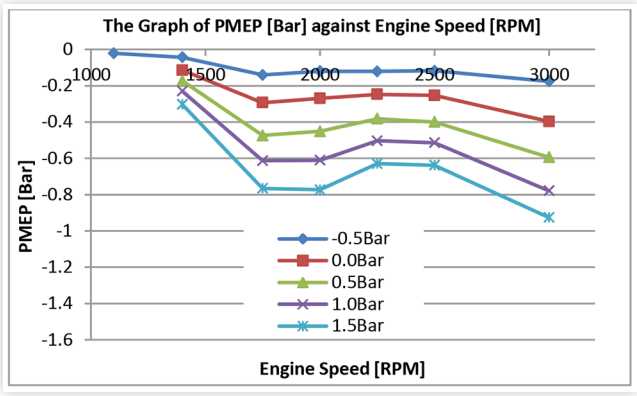

observation reaffirms the fact that the peak seen at 2000rpm in the BMEP is solely related to the volumetric efficiency of the engine, as related to the *PMEP*, and not originating from heat losses or blow-by, as measured from the $IMEP_{gross}$.

By subtracting the $IMEP_{net}$ from the BMEP, the FMEP was obtained as seen in Figure 9. Observing such relationship with engine speed it can be seen that the FMEP shows a monotonically increasing trend with an increase in engine speed as well as with load. This is consistent with physical phenomena, whereby increasing engine speed results in higher piston velocity which in turn results in higher friction footprint. On the other hand, increasing the load results in higher normal reactions between the piston and the wall as well as higher loading on the cranktrain journals, leading also to a higher FMEP. Comparing this result to that presented in the previous publication, it can be seen that a considerable difference is evident. The difference in the FMEP originates solely from the IMEP. This is attributed largely to the thermodynamic loss angle used in the computation of the IMEP in the previous publication [1].

Figure 10 shows the thermodynamic loss angle found in this work. It should be noted that during such testing the TDC probe was not installed in the combustion chamber. The location of true TDC (relative to Z-index) as calibrated by previous TDC probe testing presented at the beginning of the paper was used. Prior determining the thermodynamic loss angle, a Fast Fourier Transform was performed on the

FIGURE 9 The graph of FMEP against engine speed and load

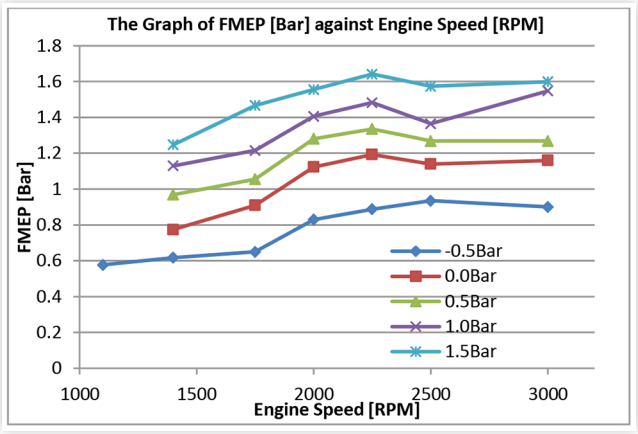

FIGURE 10 The thermodynamic loss angle for Air setpoints determined from LPP and calibrated TDC

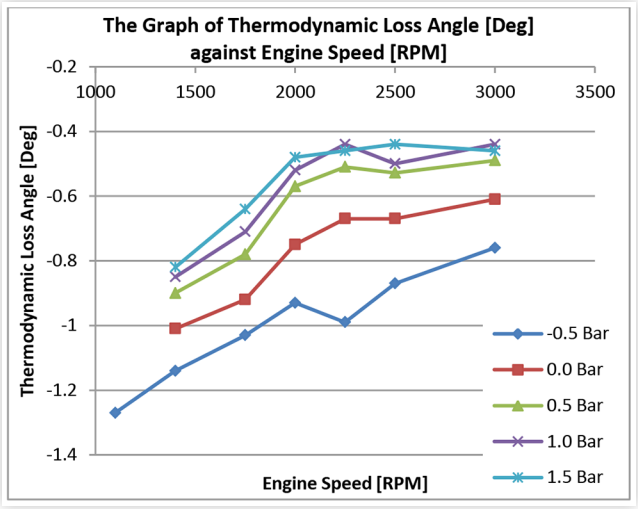

in-cylinder pressure trace, and the relevant noisy frequencies were removed to obtain a filtered trace, on which the LPP could be found for computation of the loss angle. In doing so it had to be ensured that no angular shifts were present between the filtered trace and the original unfiltered one. This was very difficult as the identification of shifts as small as ±0.1DegCA were very hard to identify due to the fluctuations present at the peak pressure in the original unfiltered traces.

From Figure 10 it is seen that the thermodynamic loss angle decreases with an increase in both engine speed and engine loading. Increasing the engine speed implies that less time is allowed for heat and blow-by to be rejected. Increasing the engine load on the other hand increases the in-cylinder gas mass. According to the polytropic law however the gas temperature and wall temperature should remain relatively the same. This implies that per unit mass of gas, there is less heat being rejected. Such two observations suggest that increasing engine speed and load approaches the adiabatic condition and hence an overall decrease in the thermodynamic loss angle.

FIGURE 11 The graph of thermodynamic loss angle as computed using Pipitone's method.

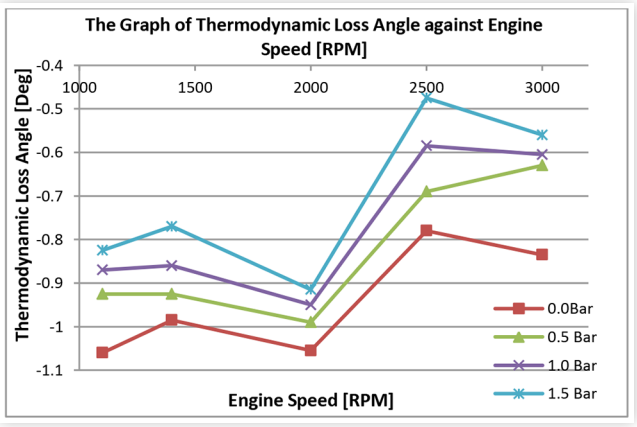

FIGURE 12 The graph of thermodynamic loss angle as computed using Stas' method.

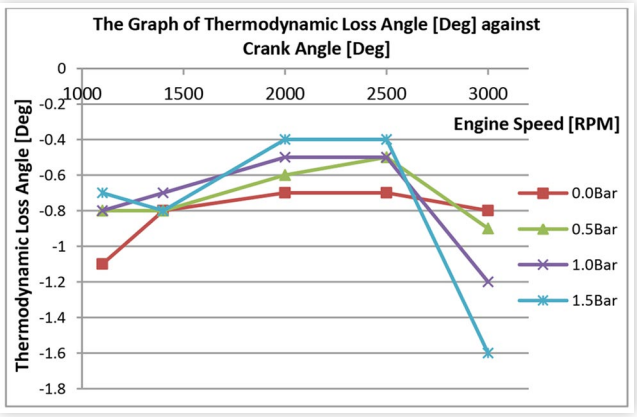

Another observation evident from Figure 10 is that beyond the 2250rpm range, the thermodynamic loss angle seems to reach a plateau. This is of course true as if this wasn't the case, then increasing the engine speed to high values might suggest that the thermodynamic loss angle would effectively be zero at some point, which is known to be physically impossible.

The data obtained in Figure 10 was compared to the loss angle found in the previous publication by using the empirical methods of Pipitone [3] and Stas' [2] given in Figure 11 and Figure 12 respectively, for the same engine on the same setup. One can identify that in general both Pipitone [3] and Stas' [2] methods seem to agree to some extent with the data communicated in Figure 10. Both methods, more evidently in that presented by Pipitone [3], the trend of decreasing loss angle with increase in engine speed and load is followed very well compared to that given in Figure 10.

Testing with Argon

After testing the engine with air, another testing session was dedicated to operating the engine on Argon. Argon was chosen in preference over any other gas due to the fact that it has one of the most different ratio of specific heats out of the commercially available gases in pressurized 100L canisters. Testing with Argon showed a very different scenario compared to that with air. Conservative manifold pressurisations had to be imposed while testing as the peak incylinder pressure rises much more than that reached with air at an equivalent manifold pressurization value. Due to this, the pressurization setpoints covered were 0.1Bar, 0.3Bar and 0.5Bar gauge pressure. It should be also noted that testing with Argon imposes very high incylinder temperatures compared to that of air. From equation 2, where subscript 1 denotes intake manifold BDC and 2 denotes compression TDC, it can be noticed that such discrepancy in temperature results solely from the ratio of specific heat capacities, while being independent of the manifold pressurization value.

$$\frac{T_2}{T_1} = \left(\frac{V_1}{V_2}\right)^{\gamma-1} \ldots \quad (2)$$

Table 5 shows the tested setpoints with respect to engine speed and load. In such testing it was noted that the engine speed was affected with a peak standard deviation of ±4rpm and mean standard deviation ±2rpm, whereas the manifold pressure showed a peak standard deviation of ±0.011Bar and mean standard deviation ±0.006Bar.

It should be noted that when testing with Argon, initially an attempt was made to use the conventional canister-mounted pressure regulator to regulate the manifold pressure. This resulted in a very unstable manifold pressure and a small tweak on the pressure regulator resulted in a very large variation in the manifold pressure. In order to solve such issue, the manual pressure regulator previously used with air pressurization was installed in series with the canister pressure regulator. With such a configuration, a two-stage pressure regulation was achieved. Such system proved to allow very fine adjustments to the manifold pressure. It should be noted by the reader that since for Argon testing, the blow-by was being rerouted to the engine, the only make-up gas that must be supplied in such case is that which leaks out, through the gaskets of the engine, which is obviously a very minute quantity.

Figure 13 shows the exhaust side shunt pipe temperature obtained with Argon. During testing, the thermocouple at the intake side of the shunt pipe failed and hence no data was recorded.

Figure 14 shows the coolant temperatures that had to be set in order to obtain an oil temperature of 80°C. It must be said that for Argon testing, setpoints at 3000rpm couldn't reach oil temperatures of 80°C, but settled at 84°C, 87°C and 88°C for 0.1Bar, 0.3Bar and 0.5Bar respectively. Such temperatures

TABLE 5 The planned test matrix for Argon testing

Setpoints Tested		Manifold Gauge Pressure [Bar] 0.1	0.3	0.5
Engine Speed [RPM]	1400	✓	✓	✓
	1750	✓	✓	✓
	2000	✓	✓	✓
	2250	✓	✓	✓
	2500	✓	✓	✓
	3000	✓	✓	✓

FIGURE 13 The shunt exhaust temperature reached while testing with Argon

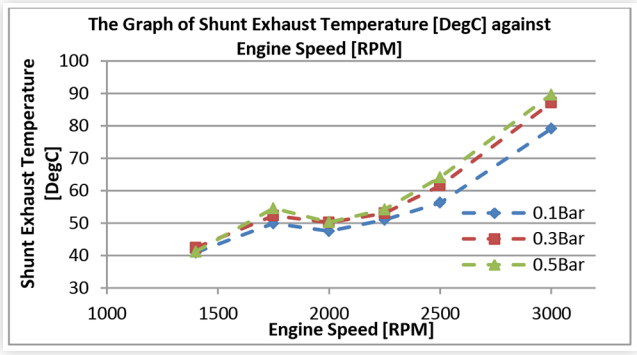

FIGURE 14 The engine coolant temperature reached during testing with Argon.

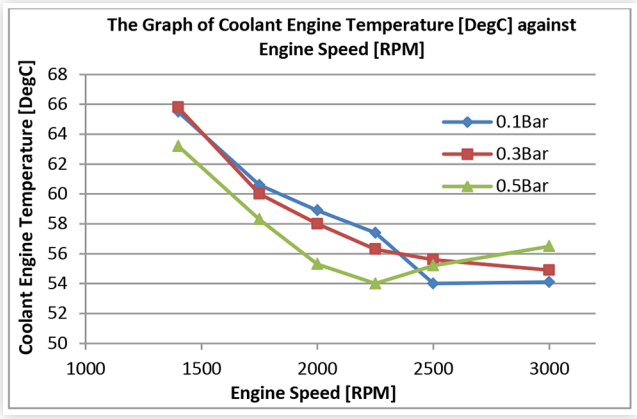

couldn't be lowered further due to the fact that the coolant temperature couldn't be lowered further than around 53°C. This was not the case when testing with Air. As seen in Figure 3, when testing with air the coolant temperature was lowered as far as 49°C. It should be noted that due to the very high incylinder temperatures reached with Argon, much larger heat transfer rates flow through the coolant, out of the engine. This implies that to lower the coolant temperature further, the coolant conditioning unit should be equipped with a larger heat exchanger, otherwise a cooler and larger mass flow rate of cooling water should be passed through the heat exchanger to be more effective in taking heat away from the coolant.

Similarly to what was seen for air testing, the peak incylinder pressure recorded with Argon and presented in Figure 15 seemed to peak at the 2000rpm region. Consequently the BMEP and IMEP shown in Figure 16 and Figure 17 respectively show a peak at around the 1750rpm - 2000rpm region as well.

Splitting up the $IMEP_{net}$ into $IMEP_{gross}$ and $PMEP$ as seen in Figure 18 and Figure 19 respectively, showed a similar observation to that seen with air, whereby the $IMEP_{gross}$ is practically linear, whereas the $PMEP$ shows a peak at around the 1750rpm due to the volumetric efficiency effects.

Computing the FMEP, given in Figure 20 showed that a very linear trend was achieved for speeds of 1750rpm upwards, whereas the FMEP at 1400rpm showed a slightly higher FMEP

FIGURE 15 The graph of peak incylinder pressure reached while testing with Argon

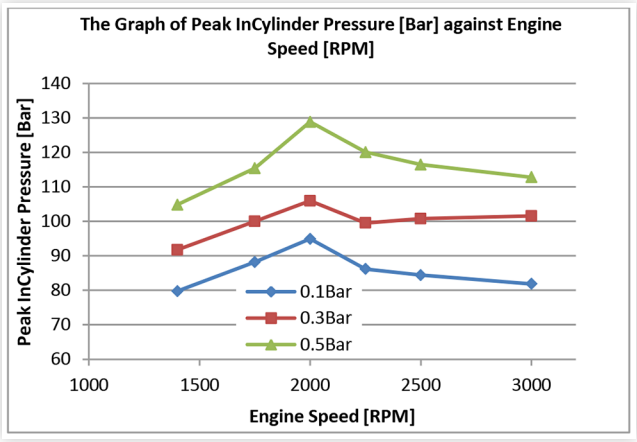

FIGURE 16 The graph of BMEP against engine speed and load with the engine operating on Argon

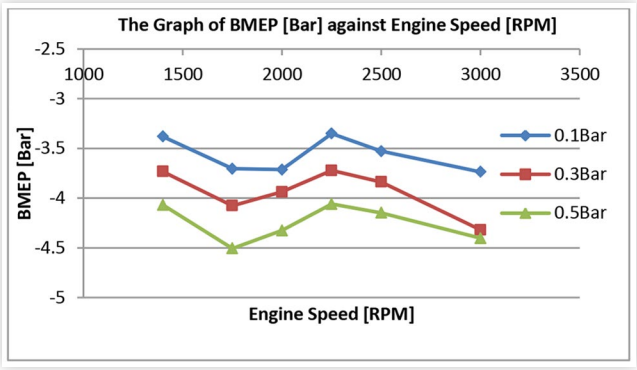

FIGURE 17 The graph of $IMEP_{net}$ against engine speed and load with the engine operating on Argon

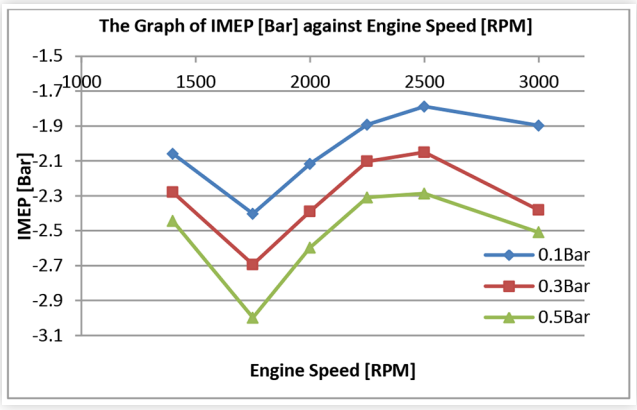

than that seen at the 1750rpm, creating a local reduction at the latter engine speed. Something worthy of attention from such result is the fact that if the trace of 0.5Bar Argon is compared with 1.5Bar Air and 0.3Bar Argon compared with 1.0Bar Air, it would show that a much larger FMEP is seen for the Argon traces. Such two loading setpoint pairs are chosen

FIGURE 18 The graph showing $IMEP_{gross}$ as a function of engine speed and load with the engine working on Argon

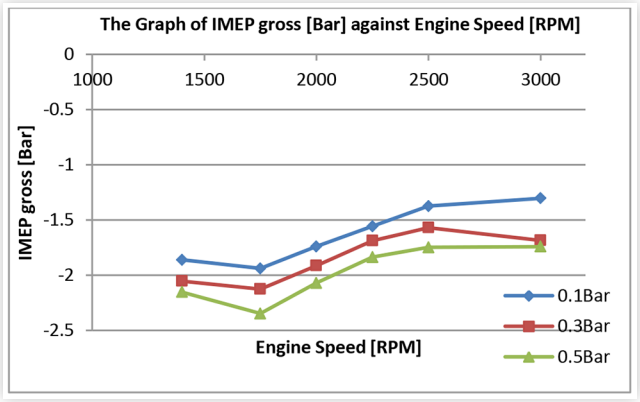

FIGURE 19 The graph of PMEP against engine speed and load for the engine working on Argon

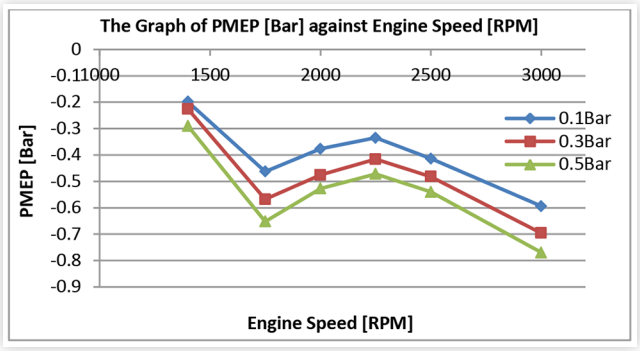

FIGURE 20 The FMEP graph for the engine operating on Argon

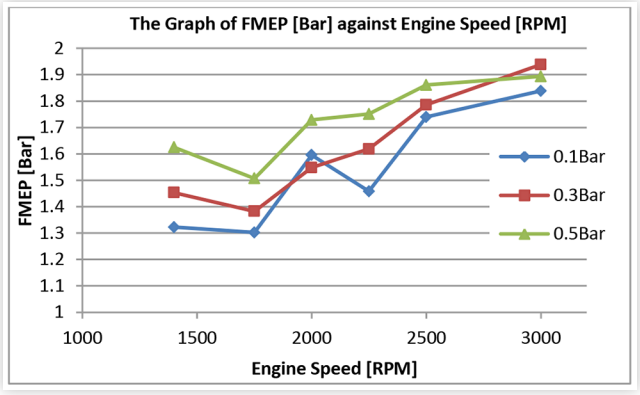

and compared based on their peak incylinder pressures, as that of 0.3Bar Argon matches that of 1.0Bar Air, and similarly with the other pair. It is the opinion of several authors like Chen and Flynn [7] that the FMEP is solely dependent on engine speed and load for an engine without accessories. This gives the impression that the FMEP of 0.3Bar Argon and 0.5Bar Argon should be very similar to 1.0Bar and 1.5Bar Air respectively. This however wasn't the case, meaning that another factor is in play. Table 6 compares the setpoints of

TABLE 6 Comparison of 1.0Bar Air and 0.3Bar Argon

	Air 2000 RPM; 1.0 Bar	Argon 2000 RPM; 0.3 Bar
BMEP [Bar]	-3.145	-3.937
IMEP net [Bar]	-1.739	-2.389
FMEP [Bar]	1.406	1.548

2000rpm; 1.0Bar Air with 2000rpm; 0.3Bar Argon to show clearly the difference in BMEP, IMEP and FMEP between such two testpoints having the same peak incylinder pressures and engine speed.

In this study a test was done whereby a bulky k-type thermocouple was inserted into the combustion chamber through the injector hole and protruding to around 0.5mm from the piston crown when the latter is at TDC. The engine was run on both Air and Argon with the thermocouple installed and steady-state readings were taken as shown in Table 7. It must be noted that since the thermocouple was not one dedicated for surface temperature measurements, it cannot be said that the temperatures in Table 7 are indeed true surface temperatures, but it can be surely argued that they are neither giving the actual gas temperature. From such test it transpired that when testing with Argon, around 200$^{\circ}C$ excess was recorded to that when tested with Air. Such high temperatures noted in the combustion chamber may lead to conditions of insufficient oil deposition on the cylinder liner, hence resulting in a higher FMEP for the Argon setpoints. Such hypothesis however is not yet backed by any other experimental evidence.

A graph of incylinder pressure versus crank angle is presented in Figure 21, whereby the ensemble average over 200 cycles is given for the 2000rpm; 0.3Bar Argon and 2000rpm; 1.0Bar Air. It is seen that along the compression stroke up to TDC, the two traces are very similar, however during the expansion stroke a lower instantaneous pressure for the Argon is evident with an excess of 5.7Bar at around 20DegCA ATDC. Such lower pressure is thought to have originated from higher heat losses when testing with Argon as compared to when testing with Air.

The loss angle found for Argon testing as given in Figure 22 seemed to show a similar relationship to that found for air, whereby the loss angle decreases with an increase in engine speed and load. It must be however said that the absolute magnitude of the loss angle for Argon is larger than that achieved for Air. This is unarguably because of the higher magnitude of heat losses originating from the combustion chamber during Argon testing, owing from higher incylinder temperatures.

TABLE 7 The steady-state wall temperature recorded a by a k-type thermocouple when testing with Air and Argon

Wall Temperature *Air [DegC]* / *Argon [DegC]*		Manifold Gauge Pressure [Bar] 0.0	0.5	1.0	1.5
Engine Speed [RPM]	1400	***194***	***193***	***197***	*n/a*
		n/a	*338*	*n/a*	*n/a*
	1750	***214***	***223***	***225***	***230***
		413	*418*	*n/a*	*n/a*

FIGURE 21 The graph of incylinder pressure against crank angle for similar load setpoints of air and argon

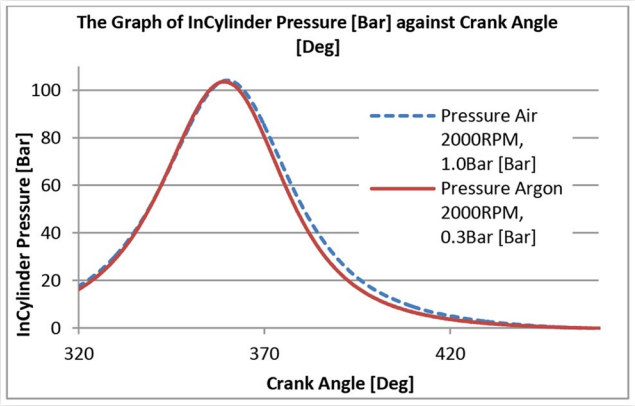

FIGURE 22 The experimentally determined thermodynamic loss angle with the engine operating on Argon

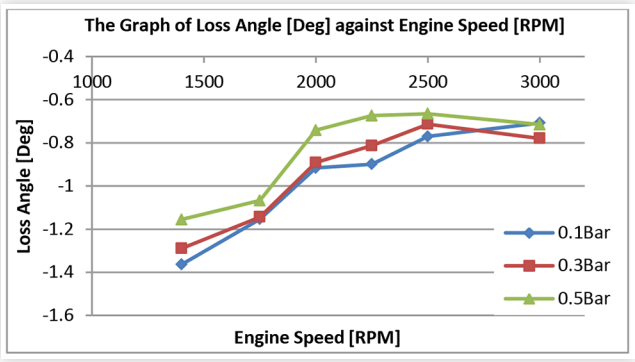

Summary and Conclusions

It is believed that in this work, the anomaly faced in the previous publication [1], where the motoring brake torque was noted to be high over the 2000rpm was better understood. It can be safely assumed that such trend was a result of the volumetric efficiency of the engine due to wave dynamics in the shunt system/trapping conditions inside the cylinder.

Thermodynamic angle is not constant but a function of speed and load (pressurisation). This was determined experimentally for both Air and Argon testing.

The trend of the experimentally derived thermodynamic loss angle has matched well with relationships observed (not in this study) under firing conditions where the heat transfer energy balance contribution increases with reduction in speed (residence time) and load (gas density).

The importance of the load effect on FMEP has been shown. Assuming that engine friction is the same at all loads (or at "atmospheric" conditions in the manifolds) can lead to more than 50 % error in FMEP at the higher engine loads.

Operation of the engine on Argon showed that very high peak pressures could be reached with relatively small manifold pressurizations. It was also noted that the thermodynamic loss angle as resulted from Argon testing was greater than that achieved when testing with Air. This is believed to have resulted from a higher heat transfer rate from the combustion chamber due to the higher bulk gas temperature on compression.

Another observation was the fact that for testpoints done with Air and Argon having the same engine speed and peak incylinder pressures, the friction mean effective pressure differed. It is hypothesized that such difference might be related to the difference in the wall temperatures which might have affected the lubricant properties as well as dimensional expansions of different engine parts in moving contact.

Having found experimentally the true TDC location of the engine proved to be of significant benefit on the data compilation. This resulted in a more linear FMEP result, as compared to that achieved in the previous publication [1]. Splitting of the $IMEP_{net}$ into $IMEP_{gross}$ and $PMEP$ showed that the shape of the $IMEP_{net}$ results largely from the PMEP, which is effectively a measure of the pumping losses.

Suggestions for Further Work

Having tested the engine with Argon highlighted the very high incylinder temperature as compared with air testing. Such quality is thought to be useful in search of obtaining accurate transient heat transfer measurements from a motored engine displaying the loading characteristics on the engine. As a result the pressurized motoring setup is being further modified in preparation for experimental testing of heat transfer determination with Air and Argon as the working medium.

Some further points to focus on in the forthcoming research are the following:

- Understanding the wave dynamics in shunt pipe system (PMEP peaks).
- Maintaining a steady coolant temperature with coolant flow to achieve a more consistent thermal condition of the engine (more consistent Oil condition at all mechanical interfaces)
- Understanding the higher FMEP when the engine's speed and peak cylinder pressures are maintained but heat transfer is modified (in this case with gas properties changed)

References

1. Caruana, C., Farrugia, M., and Sammut, G., "The Determination of Motored Engine Friction by Use of Pressurized 'Shunt' Pipe between Exhaust and Intake Manifolds," SAE Technical Paper 2018-01-0121, 2018, doi:10.4271/2018-01-0121.
2. Stas', M., "Thermodynamic Determination of T.D.C. in Piston Combustion Engines," SAE Technical Paper 960610, 1996, doi:10.4271/960610.

3. Pipitone, E. and Beccari, A., "Determination of TDC in Internal Combustion Engines by a Newly Developed Thermodynamic Approach," *Applied Thermal Engineering* 30:14, 1914-15, 1926, 2010, doi:10.1016/j.applthermaleng.2010.04.012.
4. Allmaier, H., Knauder, C., Salhofer, S., Reich, F.M. et al., "An Experimental Study of the Load and Heat Influence from Combustion on Engine Friction," *International Journal of Engine Research* 17(3):347-353, April 2015, doi:10.1177/1468087415579784.
5. Knauder, C., Allmaier, H., Salhofer, S., and Sams, T., "The Impact of Running-In on the Friction of an Automotive Gasoline Engine and in Particular on Its Piston Assembly and Valve Train," *Proceedings of the Institution of Mechanical Engineers, Part J: Journal of Engineering Tribology*, 2017, doi:1350650117727231.
6. Allmaier, H., Knauder, C., Sanders, D., and Reich, F., "Combination of Measurement and Simulation to Analyse Engine Friction," *MTZ Worldwide* 77(10):66-71, 2016.
7. Chen, S. and Flynn, P., "Development of a Single Cylinder Compression Ignition Research Engine," SAE Technical Paper 650733, 1965, doi:10.4271/650733.

Contact Information

Mario Farrugia
Mechanical Engineering Department
University of Malta, Malta
mario.a.farrugia@um.edu.mt

Carl Caruana
Mechanical Engineering Department
University of Malta, Malta.
carl.caruana.12@um.edu.mt

Acknowledgments

Throughout this study the technical and practical knowledge of Mr. Andrew Briffa and Ing. Jean Paul Azzopardi is acknowledged. Continental Corporation is thanked for the donation of the UniNOx sensor, whereas University of Palermo is thanked for giving us permission to use the TDC probe. The authors would like to thank also Ing. Noel Balzan for his help and Methode Electronics Malta for the donation of the data acquisition hardware.

The research work disclosed in this publication is partially funded by the Endeavour Scholarship Scheme (Malta). Scholarships are part-financed by the European Union-European Social Fund (ESF)-Operational Programme II-Cohesion Policy 2014-2020 "Investing in human capital to create more opportunities and promote the well-being of society".

Definitions/Abbreviations

AC - Alternating Current
BMEP - Brake Mean Effective Pressure
CI - Compression Ignition
DAQ - Data Acquisition
DegCA - Degrees of Crank Angle
FMEP - Friction Mean Effective Pressure
IMEP - Indicated Mean Effective Pressure
LPP - Location of Peak Pressure
PMEP - Pumping Mean Effective Pressure
ppr - Pulse Per Revolution
TDC - Thermodynamic Loss Angle
VFD - Variable Frequency Drive

e-ISSN 2641-9645